Thin Solid Films 596 (2015) 174–178

Contents lists available at ScienceDirect

Thin Solid Films

journal homepage: www.elsevier.com/locate/tsf

# A model for crack initiation in the Li-ion battery electrodes

Rahul Panat

*School of Mechanical and Materials Engineering, Washington State University, Pullman, WA 99164, USA*

ARTICLE INFO

*Article history:*
Received 18 May 2015
Received in revised form 16 July 2015
Accepted 24 July 2015
Available online 29 July 2015

*Keywords:*
Li-ion batteries
Surface roughening
Crack initiation
Surface diffusion
Volume diffusion
Lithiation
Si electrode
Nanostructured electrode

ABSTRACT

The development of high energy density Lithium-ion batteries is of intense interest due to their application in the electric car and consumer electronics industry. The primary limiter in using high energy density battery electrodes is the cracking of the electrode material due to the severe strain caused by the charging–discharging cycles. In this paper, a linear perturbation model is used to describe the evolution of the electrode surface under stress. The driving force for the surface undulation formation is the reduction in the electrode strain energy. The kinetics of mass transport is described by the surface and volume diffusion. The model predicts that the Si electrode will develop surface undulations of the order of sub-1 μm length scale on the electrode surface, showing a reasonable agreement with experimental results reported in literature. Such surface undulations roughen the anode surface and can form notches that can act as crack initiation sites. It is also shown that this model is applicable when the temperature of the system is not constant and the system is not isolated. The limitations of the model are also discussed.



## 1. Introduction

The desire to achieve the highest possible time-between-charging for the electronic devices as well as the desire to reduce the fossil fuel usage is driving the development of high energy density Li-ion batteries [1]. A great deal of current research on the Li-ion batteries has concentrated on identifying novel electrode and electrolyte materials. Amongst the various material candidates for the Li-ion batteries, silicon (Si) is of particular interest as an anode due to its very high theoretical charge capacity (4200 mAh/g) [2] along with its abundance in earth's crust. Although the capacity of Si electrode is about 10 times higher than the commercially used material graphite, Si undergoes large (~350 to 400%) volume expansion during charging cycle resulting in electrode pulverization and early capacity fade [3]. Several nano-geometries have been explored to overcome this problem in the form of nano-rods on a plane [4,5]; Si–C core shell nanostructures [6,7], Si nanotubes [8], Si nano films with [9] or without [10–15] soft substrates, hollow nanospheres [16], and coated nano-rods [17,18]. Although the nano-structured electrodes help accommodate the strain and prevent the build-up of stresses, the total electrode volume available in these cases, however, is limited primarily due to the low total volume of the nanostructures.

The major obstacle in using high energy density electrode materials (Si or otherwise) is the cracking and the resulting pulverization of the electrode due to high deformation during lithiation. This process involves crack initiation at the electrode surface or interior and its growth under the mechanical forces [3,19–21]. Several studies have been carried out to find a critical crack size and its growth in lithiated Si. Suo and co-workers [22–25] studied combined diffusion and the resulting stress accumulation at high and low charging rates. They also modeled the inelastic deformation in Si considering diffusion, elastic–plastic deformation, and fracture. Chiang and co-workers [26,27] have created an electrochemical shock map that shows the regime of failure depending upon the charging rate, particle size, and the inherent fracture toughness of the material. They also showed that minimizing the principal shear strain, rather than minimizing net volume change as previously suggested, is an important new design criterion for crystal chemical engineering of electrode materials for mechanical reliability. Medium range order in disordered Si is an important consideration for crack propagation in the electrodes [28–30]. Fluctuation electron microscopy experiments along with simulations have established a medium range orientational order in amorphous silicon [28,29]. This medium range order, as described by paracrystalline models, consists of topologically crystalline grains which are strongly strained and a disordered matrix between them [28]. Verbrugge and co-workers [31–33] have proposed a tensile stress-based criteria for the growth of cracks within a spherical insertion electrode. They considered both interfacial (electrochemical) kinetics and intercalate diffusion. Gao and co-workers [34,35] developed a cohesive model of crack nucleation in an initially crack-free strip electrode under galvanostatic intercalation and de-intercalation processes. They applied a cohesive zone model of crack nucleation in a cylindrical electrode under axisymmetric diffusion induced stresses. The cracks were assumed to exist at a certain

*E-mail address:* rahul.panat@wsu.edu.

http://dx.doi.org/10.1016/j.tsf.2015.07.066
0040-6090/

periodicity. The above models provide an excellent picture of the *crack growth* in a battery electrode under lithiation stresses. The exact mechanisms of how the surface cracks evolve from surface features, however, have not been fully investigated.

Li et al. [3] have observed that a flat bulk Si anode surface develops a characteristic surface roughness at a length scale of <1 μm upon lithiation. They observed that some surface cracks grow to form a fractal pattern at a higher length scale of tens of micrometers. Note that they observed that the Si surface roughness/undulations grow with time upon lithiation, although the amplitude and the dominant wavelength were not quantitatively characterized. Such sub-micron surface features can potentially act as crack initiation sites. Similar to the bulk silicon, the nanostructured Si anodes are also shown to form surface undulations upon lithiation. Direct TEM observations of Si nano-rod anodes undergoing lithiation [36] show clear Si surface undulations at a wavelength of about 100–200 nm and an amplitude of about tens of nm (Fig. 3d in Ref. [36]).

In this communication, we develop a linear perturbation model to describe the formation and evolution of surface undulations in Li-ion battery electrode films under stress caused by Li intercalation. The formulation takes into account the fact that the Li-ion battery electrode is not an isolated system and that the temperature can change during lithiation. Additionally, no assumptions are made regarding pre-existing flaws on the surface. It is shown that the formulation follows the description of the rumpling problem in metallic thin films previously addressed by the author [37]. A competition between surface energy and strain energy is shown to be the driver for the mass transport. The kinetics of mass transport is described by surface and volume diffusion. The model predicts that the surface undulations with 0.2 to 1 μm wavelength grow at the highest rate and dominate the surface in a reasonable agreement with experimental results from literature [3,36]. These undulations can give rise to notches that can act as crack initiation sites. Implications of the model in terms of the microstructural evolution at or near the surface of the battery electrode are discussed. Finally, the limitations of the model are discussed in detail.

## 2. Model

Consider a battery electrode film of Si as shown in Fig. 1. Consider for the time being that the Si is polycrystalline (i.e. diffusion is isotropic) and that the usual chemical potentials are driving the Li inside the electrode during charging cycle. As the charging goes on, the Si film will go under compressive stress during lithiation. The high diffusivity of the Li material inside and on the surface of Si, however, can give rise to some surface rearrangements driven by the desire to lower the free energy. To describe the roughness formation, the surface of the electrode can be decomposed into infinitely many sinusoidal undulations. The assumption is that we analyze each wave independently and the resultant surface is linear superposition of the waves. A single surface perturbation of wavelength is $h(x, t) = a(t)\cos(\omega x)$, with $\omega = 2/\lambda$ (Fig. 1b). The actual surface profile can be described as, $\sum_{k=1}^{\infty} a_k \cos(\omega_k x)$.

For a semi-infinite body of unit depth under a remote stress (Fig. 1b), the strain energy density in the body per unit volume is $U(\varepsilon_{ij})$. The internal energy of the system is comprised of the strain energy and surface energy, i.e.,

$$\varepsilon = \int_V U(\varepsilon_{ij})dV + \int_S \gamma\, dS. \tag{1}$$

The system free energy is,

$$F = \varepsilon - \int_V Ts(V)\, dV, \tag{2}$$

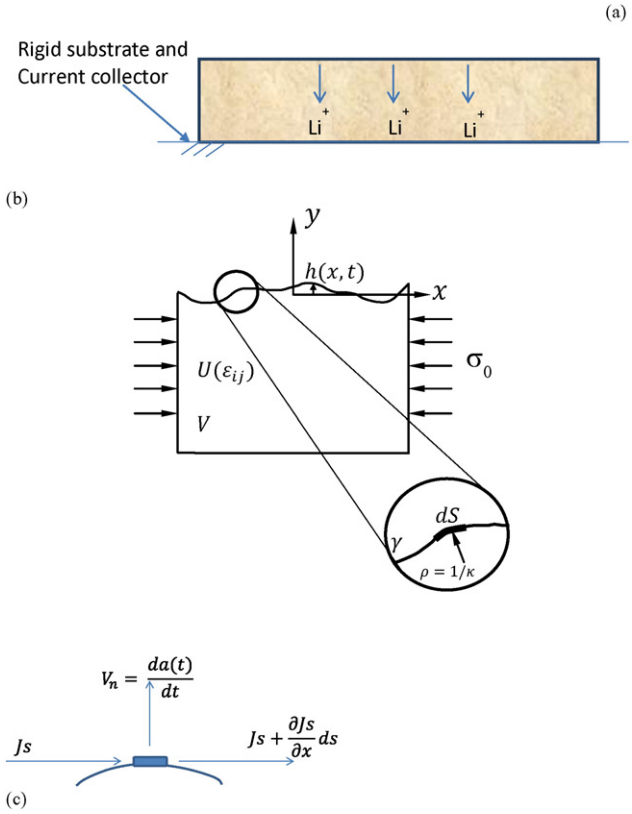


**Fig. 1.** (a) Li diffusion normal to the electrode surface driven by battery chemical potential, (b) surface of a battery film under compressive residual stresses, and (c) conservation of volume at the surface.

where '$s(V)$' is the local entropy and T is the total absolute temperature of the solid. From Eqs. (1) and (2),

$$F = \int_V U(\varepsilon_{ij})dV + \int_S \gamma\, dS - \int_V Ts(V)\, dV. \tag{3}$$

The time rate change of the free energy is,

$$\dot{F} = \int_V \frac{\partial U(\varepsilon_{ij})}{\partial t}dV + \int_V U(\varepsilon_{ij})\frac{\partial\,(dV)}{\partial t} + \int_S \frac{\partial \gamma}{\partial t}\, dS + \int_S \gamma\, \frac{\partial (dS)}{\partial t} - \int_V \frac{\partial T}{\partial t} s(V)dV - \int_V T\frac{\partial s(V)}{\partial t}\, dV - \int_V Ts(V)\frac{\partial (dV)}{\partial t}. \tag{4}$$

In writing Eq. (4), it is assumed that the spatial gradients of $U$ and $T$ are negligible compared with their time variations. The spatial gradient of $U$ can be ignored if the surface stress is uniform, while for a thin layer such as a battery electrode, the spatial gradient of $T$ can be ignored if the heat conduction is fast enough to make the gradients insignificant. A simple derivation [38,39] shows that,

$$\int_S \gamma\, \frac{\partial (dS)}{\partial t} = -\int_S \kappa\, \gamma\, V_n\, dS. \tag{5}$$

Furthermore, for small perturbations of the surface, the strain energy change in the bulk is negligible compared to that on the surface. Hence,

$$\int_V U(\varepsilon_{ij})\frac{\partial (dV)}{\partial t} = \int_S U(\varepsilon_{ij})\, V_n\, \mathrm{d}S\,. \tag{6}$$

Similarly,

$$\int_V Ts\frac{\partial(dV)}{\partial t} = \int_S T\,s\,V_n \mathrm{d}S. \tag{7}$$

Note that the above system is not in thermodynamic equilibrium. From Eqs. (4), (5), (6), and (7), we obtain

$$0 = \int_V \frac{\partial U(\varepsilon_{ij})}{\partial t} dV + \int_S \frac{\partial \gamma}{\partial t}\, dS - \int_V \frac{\partial T}{\partial t} s(V) dV - \int_V T\frac{\partial s(V)}{\partial t}\, dV. \tag{8}$$

From Eqs. (**4**) and (**8**), we obtain,

$$\dot{F} = \int_S \left(U(\varepsilon_{ij}) - \kappa\,\gamma - T\,s\right) V_n\, \mathrm{d}S. \tag{9}$$

The factor $V_n \mathrm{d}S$ is equal to the atomic volume, Ω, times the atomic flux at d$S$. The chemical potential, $\chi$, along the surface of the solid can be obtained from Eq. (9) as,

$$\chi = \left(U(\varepsilon_{ij}) - \kappa\,\gamma - T\,s\right)\Omega, \tag{10}$$

where $U$ is the strain energy density along the film surface. Here $\kappa$ is the curvature ($= \partial^2 h(x,t)/\partial x^2$), $\gamma$ is the surface energy and Ω is the atomic volume. The value of $\frac{\partial \chi}{\partial x}$ is of interest since it represents the gradient in the surface chemical potential. Although the system is not in thermodynamic equilibrium, the relation $ds = dq/T$ is valid at every point along the solid surface (due to local thermodynamic equilibrium). The term $dq$ represents the local change in the heat energy and is equal to $C_p dT$, with $C_p$ being the heat capacity of the solid. We can then write,

$$Ts = T\int_{T_{ref}}^{T} \frac{C_p dT'}{T'} = C_p\, T \ln\left(\frac{T}{T_{ref}}\right). \tag{11}$$

Eq. (11) is very important in determining the effect of entropy change on the system as the surface waviness is formed. From Eq. (11), if the temperature along the solid surface is constant at a given moment, we take $\partial(Ts)/\partial x = 0$ ($C_p$ is taken to be constant). Thus, the entropy term is shown not to contribute to the surface gradient of the chemical potential as given by Eq. (10). The problem formulation thus reverts back to that developed previously by the author and others [37–40] and is described below for clarity.

Note that the stress at the surface due to a 'small' perturbation of amplitude '$a$' and wavelength 'λ' is: [41–43]

$$\sigma_{xx}(x,\, y=0) = \sigma_0 - 2\sigma_0 a\omega\cos(\omega x). \tag{12}$$

Where $\sigma_0$ is the remote stress caused by lithiation. Eq. (12) gives rise to strain energy density,

$$U(x,t) = \left[\frac{(1-\nu)\sigma_0^2}{4G}\right][1 - 4a\omega\cos(\omega x)]. \tag{13}$$

The –ve sign indicates reduction in strain energy density due to undulation.

The flux of the atoms along the surface is proportional to the chemical potential gradient given by Eq. (10),

$$Js = \frac{-D_s C_s}{kT}\frac{\partial\left(U(\varepsilon_{ij}) - \kappa\,\gamma - T\,s\right)}{\partial x} = \frac{-D_s C_s \Omega \sin(\omega x)}{kT}\left[\frac{(1-\nu)\sigma_0^2}{G}\, a\omega^2 - \gamma a\omega^3\right]. \tag{14}$$

The normal velocity of the surface will then be $-\Omega\left(\frac{\partial Js}{\partial x}\right)$ (Fig. 1-c), giving,

$$\frac{da(t)}{dt} = \frac{D_s C_s \Omega^2 \mathrm{a(t)}}{kT}\left[\frac{(1-\nu)\sigma_0^2}{G}\,\omega^3 - \gamma\omega^4\right]. \tag{15}$$

From Eq. (15), the rate of growth of perturbation amplitude of the wave is dependent upon the amplitude itself. The first term in the bracket is the strain energy term that increases the wavelength while the second term is the surface energy term that will try to smoothen the surface. The dependence of the first term is $1/\lambda^3$, while that for the second term is $1/\lambda^4$.

The diffusivity of Li on Si surfaces as well as surface Li concentration has not been measured. The only measurement of $D_s C_s$ for Li was at room temperature in ultra-high vacuum on graphite [44]. The diffusivity, $D_s$ at 300 K was $5 \times 10^{-6}$ cm$^2$/s, the activation energy was 0.16 +/− 0.02 eV, and $C_s$ was $8 \times 10^{14}$ atoms/cm$^2$. This is very low activation energy and at room temperature, a very high $D_s$ value. For comparison, the activation energy for surface self-diffusion of Ni is 1.5–1.8 eV, while $D_s$ at 1300 K is $3 \times 10^{-6}$ cm$^2$/s. The $D_s C_s$ in Ref. [44] was calculated in ultra-high vacuum, while in the actual battery electrodes this value is expected to be lower by a few orders of magnitude due to surface contaminants.

The volume diffusion of Li in Si can also give rise to Si surface roughening. The expression for surface evolution due to vacancy diffusion was derived by the author previously as [37],

$$\frac{da(t)}{dt} = \frac{D_1 \Omega\, \mathrm{a(t)}}{kT}\left[\frac{2(1+\nu)\sigma_0}{3}\,\omega^2 - \gamma\omega^3\right]. \tag{16}$$

Where $D_1$ is the volume self-diffusivity of the solid. The first term has $1/\lambda^2$ dependence on $da/dt$, similar to 1/(grain size) [2] dependence in creep. The diffusivity of Li in Si has been calculated by several recent studies at room temperature to be about $10^{-12}$ to $10^{-13}$ cm$^2$/s (Ref. [45]). We approximate $D_1$ to be this value and evaluate between the measured range of values. A combination of surface and volume diffusion is combined to get the final expression for rate of amplitude growth for a given surface undulation:

$$\frac{da(t)}{dt} = \frac{D_s C_s \Omega^2 a(t)}{kT}\left[\frac{(1-\nu)\sigma_0^2}{G}\omega^3 - \gamma\omega^4\right] + \frac{D_1 \Omega\, a(t)}{kT}\left[\frac{2(1+\nu)\sigma_0}{3}\,\omega^2 - \gamma\omega^3\right]. \tag{17}$$

We integrate Eq. (17), to get the following time dependent evolution equation.

$$\mathrm{Ln}\left[\frac{a(t)}{a(0)}\right] = \left\{\frac{8\pi^3 D_s C_s \sigma_0^6 \Omega^2 \mathrm{t}}{kT\gamma^3 G^3}\right\}\left[\frac{\omega\gamma G}{2\pi\sigma_0^2}\right]^3 \times \left[\frac{(1-\nu)\sigma_0^2}{G} - \gamma\omega + \frac{D_1}{D_s C_s \Omega}\frac{2(1+\nu)\sigma_0}{3\omega} - \frac{D_1}{D_s C_s \Omega}\gamma\right]. \tag{18}$$

Here, $2\pi\sigma_0^2/\omega\gamma G$, represents dimensionless wavelength. The terms in the curly bracket will be taken on the LHS since we are interested in determining the relative rate of each perturbation and plotted as normalized growth rate (see next section).

## 3. Discussion

Figs. 2(a) and (b) show the growth of the amplitude of perturbations for different perturbation wavelengths for parameters noted in Table 1 and a compressive stress of 2 GPa and 1 GPa, respectively. Note that in the case of a battery electrode (Table-1), the contribution from all the four smoothing and roughening mechanisms given by Eq. (18) is

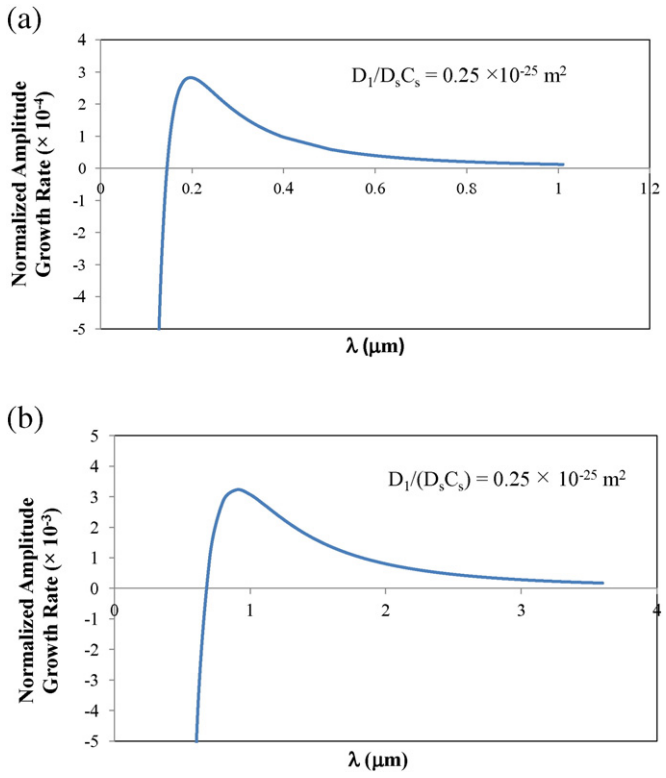


**Fig. 2.** Rate of growth for different surface perturbation wavelengths. (a) for 2 GPa stress and (b) for 1 GPa stress.

significant, unlike the case for thick films at low stresses observed in thermal barrier systems [37]. For 2 GPa stress in the film, we see that the surface perturbations with waviness less than 0.18 μm decay in amplitude with time, while perturbations with waviness close to about 0.2–0.4 μm grow at a very fast rate. For longer wavelengths, the amplitude grows very slowly at $\lambda > 0.6$ μm. For a stress of 1 GPa (Fig. 2b), the eventual dominant wavelength over the surface is predicted to be about 1 μm. The sub-μm dominant surface features observed in experiments [3,36] are very close to that predicted by the current formulation.

Fig. 3 shows the maximum wavelength as a function of $D_1/D_sC_s$ for different film stress. The max wavelength increases with decreasing stress, indicating that the dominant wavelength moves to larger values with lower stresses, but the rate of growth drops down. All the direct observations of the lithiation point to a stress of the level of 1–2 GPa in bulk materials [19,20]. Even for nanostructured Si anodes over a

**Table 1**
Material properties used to calculate the surface waviness formation in Si electrodes of the Li-ion batteries.

| Parameter | Value | Reference/Comment |
|---|---|---|
| $G$ | 80 GPa | From [46]. Value for host Si. |
| $\nu$ | 0.27 | |
| $\gamma$ | 1 J/m² | |
| $\sigma_0$ | 0.5–2 GPa | Max value taken from Ref [3]. The measured value from Ref [20] is 1.7 GPa. |
| $D_1$ | $10^{-12}$ to $3 \times 10^{-14}$ cm²/s | Ref [45] |
| $DsCs$ | $D_s = 5 \times 10^{-6}$ cm²/s<br>$C_s = 8 \times 10^{14}$ atoms/cm²<br>Giving $D_sC_s = 4 \times 10^9$ atoms/s | Value measured in ultra-high vacuum on graphite [44]. In real batteries, diffusivity will be few orders of magnitude less due to surface contaminants etc. No value available for Li diffusion on Si surface. |
| $D_1/D_sC_s$ | Range evaluated from $0.25 \times 10^{-23}$ m² to $0.25\ 10^{-27}$ m² | |
| $\Omega$ | $1.4139 \times 10^{-29}$ | Assuming Li atomic radius of $0.15 \times 10^{-9}$ m |

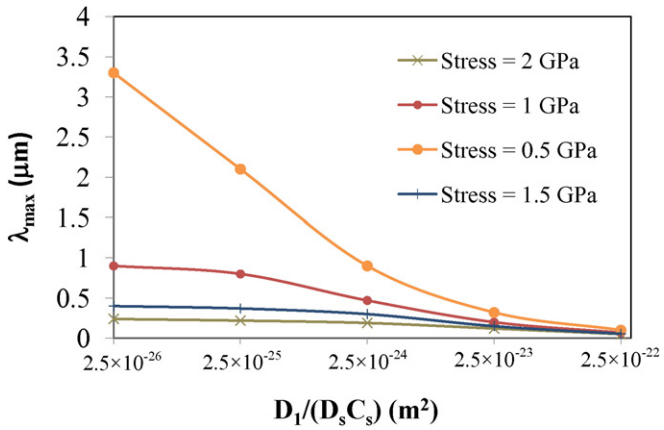


**Fig. 3.** The $\lambda_{max}$ for different volume to surface diffusivity ratios at different stress levels.

soft substrates, the anode stress have been calculated to be of the order of 1 GPa [9]. Note that although we have taken the stress to be compressive in the current formulation, the max wavelength is not affected significantly by the sign of the stress. Note also that in the absence of stress (or even for low stress), the surface roughening cannot happen since the surface energy increase will dominate over the strain energy decrease during roughening. Only surface smoothing can happen in such cases. The results also point to the fact that already undulating surfaces of a battery electrode can help in stress relaxation and avoid crack initiation at the surfaces.

From Fig. 2, it is clear that the perturbations with wavelengths in a small range of values will dominate the surface once enough time is given for the surface to evolve. For the perturbations smaller than the critical wavelength, the surface energy dominates and the amplitude dies down. For large wavelength perturbations, the time scale is too large before any meaningful amplitude increase can happen. It is noted that once the amplitude is large compared to the wavelength, the small scale assumption is no longer valid and the present formulation is not applicable. In addition, if the thermal conductivity of the electrode material is poor, the assumption of the surface gradient of *Ts* being small is not valid either. Although the current formulation assumes that the Li atoms move through Si bulk and help create the waviness, we note that the breakdown of Si structure during intercalation may result in Si atoms contributing to the roughening process as well. The medium range order in amorphous Si can also affect crack propagation [30] and not considered in the current formulation. Clearly, critical experiments are needed to observe the diffusive processes at or near the electrode surface in order to gain a full understanding of this phenomenon in the Li-ion batteries. Lastly, we note that if Li is not cleaned properly from the electrode surface in the dry box after battery disassembly, several electrochemical features associated with the SEI layer are formed over the electrode surface that can prevent clean experiments to observe the surface roughening. In spite of the several limitations discussed above, the present formulation provides a highly useful insight into a possible crack initiation mechanism during the electrochemical fatigue in battery electrode films.

## 4. Conclusion

In this paper, a linear perturbation model is applied to the crack initiation problem in Li-ion battery electrodes undergoing lithiation–delithiation cycles. The driving force for the surface undulation formation is the reduction in the electrode strain energy. The kinetics of mass transport is described by the surface and volume diffusion. The model allows the temperature of the battery to change and does not require the system to be isolated. The Si electrode is predicted to develop surface undulations of the order of sub-1 μm length scale on the electrode surface in a reasonable agreement with experimental results

reported in literature. Such surface undulations roughen the electrode surface and can form notches that can act as crack initiation sites. It is also shown that this model is applicable when the temperature of the system is not constant and the system is not isolated. The limitations of the model are also discussed.

## 5. List of symbols

| | |
|---|---|
| $\boldsymbol{h}(\boldsymbol{x}, \boldsymbol{t})$ | height of perturbation |
| $\boldsymbol{a}(\boldsymbol{t})$ | amplitude of perturbation |
| $\boldsymbol{\omega}$ | perturbation frequency associated with wavelength $\boldsymbol{\lambda}$ |
| $\boldsymbol{U}(\boldsymbol{\varepsilon_{ij}})$ | electrode strain energy density |
| $\gamma$ | electrode surface energy |
| $s(V)$ | local entropy |
| $T$ | electrode temperature |
| $V_n$ | normal velocity of the electrode surface |
| $\Omega$ | atomic volume for the diffusing species |
| $\chi$ | electrode surface chemical potential |
| $C_p$ | heat capacity of the electrode |
| $\sigma_0$ | remote stress in the electrode caused by lithiation |
| $\nu$ | Poisson's ratio for the electrode |
| $G$ | shear modulus of the substrate |
| $Js$ | flux of the atoms along the surface |
| $\boldsymbol{D_s}$ | surface diffusivity of diffusing species |
| $\boldsymbol{C_s}$ | surface concentration of diffusing species |
| $D_1$ | volume diffusivity of diffusing species |

## Acknowledgment

The work was supported by the WSU startup funds for RP. Helpful discussions with Prof. K. Jimmy Hsia are acknowledged.

## References

[1] E. Moniz, Strategic Plan 2014–2018, Department of Energy 2014, pp. 1–23.
[2] B. Boukamp, G. Lesh, R. Huggins, All-solid lithium electrodes with mixed-conductor matrix, J. Electrochem. Soc. 128 (1981) 725–729.
[3] J. Li, A.K. Dozier, Y. Li, F. Yang, Y.-T. Cheng, Crack pattern formation in thin film lithium-ion battery electrodes, J. Electrochem. Soc. 158 (2011) A689–A694.
[4] C.K. Chan, et al., High-performance lithium battery anodes using silicon nanowires, Nat. Nanotechnol. 3 (2007) 31–35.
[5] B. Liu, et al., Hierarchical silicon nanowires–carbon textiles matrix as a binder-free anode for high-performance advanced lithium-ion batteries, Sci. Rep. 3 (2013).
[6] X.-y. Zhou, J.-j. Tang, J. Yang, J. Xie, L.-l. Ma, Silicon@ carbon hollow core–shell heterostructures novel anode materials for lithium ion batteries, Electrochim. Acta 87 (2013) 663–668.
[7] Y. Ru, D.G. Evans, H. Zhu, W. Yang, Facile fabrication of yolk–shell structured porous Si–C microspheres as effective anode materials for Li-ion batteries, RSC Adv. 4 (2014) 71–75.
[8] M.H. Park, et al., Silicon nanotube battery anodes, Nano Lett. 9 (2009) 3844–3847, http://dx.doi.org/10.1021/nl902058c.
[9] C. Yu, et al., Silicon thin films as anodes for high-performance lithium-ion batteries with effective stress relaxation, Adv. Energy Mater. 2 (2012) 68–73.
[10] L.B. Chen, J.Y. Xie, H.C. Yu, T.H. Wang, An amorphous Si thin film anode with high capacity and long cycling life for lithium ion batteries, J. Appl. Electrochem. 39 (2009) 1157–1162, http://dx.doi.org/10.1007/s10800-008-9774-1.
[11] T. Zhang, et al., The structural evolution and lithiation behavior of vacuum-deposited Si film with high reversible capacity, Electrochim. Acta 53 (2008) 5660–5664, http://dx.doi.org/10.1016/j.electacta.2008.03.017.
[12] J. Graetz, C.C. Ahn, R. Yazami, B. Fultz, Highly reversible lithium storage in nanostructured silicon, Electrochem. Solid-State Lett. 6 (2003) A194–A197, http://dx.doi.org/10.1149/1.1596917.
[13] H.J. Jung, M. Park, S.H. Han, H. Lim, S.K. Joo, Amorphous silicon thin-film negative electrode prepared by low pressure chemical vapor deposition for lithium-ion batteries, Solid State Commun. 125 (2003) 387–390.
[14] K.L. Lee, J.Y. Jung, S.W. Lee, H.S. Moon, J.W. Park, Electrochemical characteristics of a-Si thin film anode for Li-ion rechargeable batteries, J. Power Sources 129 (2004) 270–274, http://dx.doi.org/10.1016/j.jpowsour.2003.10.013.
[15] S. Bourderau, T. Brousse, D.M. Schleich, Amorphous silicon as a possible anode material for Li-ion batteries, J. Power Sources 81 (1999) 233–236.
[16] Y. Yao, et al., Interconnected silicon hollow nanospheres for lithium-ion battery anodes with long cycle life, Nano Lett. 11 (2011) 2949–2954.
[17] T. Song, et al., Arrays of sealed silicon nanotubes as anodes for lithium ion batteries, Nano Lett. 10 (2010) 1710–1716.
[18] L.F. Cui, R. Ruffo, C.K. Chan, H.L. Peng, Y. Cui, Crystalline-amorphous core-shell silicon nanowires for high capacity and high current battery electrodes, Nano Lett. 9 (2009) 491–495, http://dx.doi.org/10.1021/nl8036323.
[19] M.J. Chon, V.A. Sethuraman, A. McCormick, V. Srinivasan, P.R. Guduru, Real-time measurement of stress and damage evolution during initial lithiation of crystalline silicon, Phys. Rev. Lett. 107 (2011) 045503.
[20] V.A. Sethuraman, M.J. Chon, M. Shimshak, V. Srinivasan, P.R. Guduru, In situ measurements of stress evolution in silicon thin films during electrochemical lithiation and delithiation, J. Power Sources 195 (2010) 5062–5066.
[21] J.W. Choi, Y. Cui, W.D. Nix, Size-dependent fracture of Si nanowire battery anodes, J. Mech. Phys. Solids 59 (2011) 1717–1730.
[22] K. Zhao, M. Pharr, J.J. Vlassak, Z. Suo, Inelastic hosts as electrodes for high-capacity lithium-ion batteries, J. Appl. Phys. 109 (2011) 016110.
[23] K. Zhao, M. Pharr, S. Cai, J.J. Vlassak, Z. Suo, Large plastic deformation in high-capacity lithium-ion batteries caused by charge and discharge, J. Am. Ceram. Soc. 94 (2011) s226–s235.
[24] K. Zhao, M. Pharr, L. Hartle, J.J. Vlassak, Z. Suo, Fracture and debonding in lithium-ion batteries with electrodes of hollow core–shell nanostructures, J. Power Sources 218 (2012) 6–14.
[25] Y. Hu, X. Zhao, Z. Suo, Averting cracks caused by insertion reaction in lithium-ion batteries, J. Mater. Res. 25 (2010) 1007–1010.
[26] W.H. Woodford, Y.-M. Chiang, W.C. Carter, "Electrochemical shock" of intercalation electrodes: a fracture mechanics analysis, J. Electrochem. Soc. 157 (2010) A1052–A1059.
[27] W.H. Woodford, Y.-M. Chiang, W.C. Carter, Electrochemical shock in ion-intercalation materials with limited solid-solubility, J. Electrochem. Soc. 160 (2013) A1286–A1292.
[28] P. Voyles, et al., Structure and physical properties of paracrystalline atomistic models of amorphous silicon, J. Appl. Phys. 90 (2001) 4437–4451.
[29] S. Khare, S. Nakhmanson, P. Voyles, P. Keblinski, J. Abelson, Evidence from atomistic simulations of fluctuation electron microscopy for preferred local orientations in amorphous silicon, Appl. Phys. Lett. 85 (2004) 745–747.
[30] S.N. Bogle, P.M. Voyles, S.V. Khare, J.R. Abelson, Quantifying nanoscale order in amorphous materials: simulating fluctuation electron microscopy of amorphous silicon, J. Phys. Condens. Matter 19 (2007) 455204.
[31] Y.-T. Cheng, M.W. Verbrugge, Diffusion-induced stress, interfacial charge transfer, and criteria for avoiding crack initiation of electrode particles, J. Electrochem. Soc. 157 (2010) A508–A516.
[32] Y.-T. Cheng, M.W. Verbrugge, The influence of surface mechanics on diffusion induced stresses within spherical nanoparticles, J. Appl. Phys. 104 (2008) 083521.
[33] R. Deshpande, Y.-T. Cheng, M.W. Verbrugge, Modeling diffusion-induced stress in nanowire electrode structures, J. Power Sources 195 (2010) 5081–5088.
[34] T.K. Bhandakkar, H. Gao, Cohesive modeling of crack nucleation in a cylindrical electrode under axisymmetric diffusion induced stresses, Int. J. Solids Struct. 48 (2011) 2304–2309.
[35] T.K. Bhandakkar, H. Gao, Cohesive modeling of crack nucleation under diffusion induced stresses in a thin strip: Implications on the critical size for flaw tolerant battery electrodes, Int. J. Solids Struct. 47 (2010) 1424–1434.
[36] X.H. Liu, et al., In situ atomic-scale imaging of electrochemical lithiation in silicon, Nat. Nanotechnol. 7 (2012) 749–756.
[37] R. Panat, K.J. Hsia, D.G. Cahill, Evolution of surface waviness in thin films via volume and surface diffusion, J. Appl. Phys. 97 (2005) 013521.
[38] Freund, L., Beltz, G. & Jonsdottir, F. in MRS Proceedings. 383 (Cambridge Univ. Press)
[39] L. Freund, F. Jonsdottir, Instability of a biaxially stressed thin film on a substrate due to material diffusion over its free surface, J. Mech. Phys. Solids 41 (1993) 1245–1264.
[40] H. Gao, Some general properties of stress-driven surface evolution in a heteroepitaxial thin film structure, J. Mech. Phys. Solids 42 (1994) 741–772.
[41] R. Asaro, W. Tiller, Interface morphology development during stress corrosion cracking: Part I. Via surface diffusion, Metall. Trans. 3 (1972) 1789–1796.
[42] P. Vasudev, R. Asaro, W. Tiller, Interface morphology development during stress corrosion cracking—II. Via volume diffusion, Acta Metall. 23 (1975) 341–344.
[43] H. Gao, Stress concentration at slightly undulating surfaces, J. Mech. Phys. Solids 39 (1991) 443–458.
[44] L. Mandeltort, J.T. Yates Jr., Rapid atomic Li surface diffusion and intercalation on graphite: a surface science study, J. Phys. Chem. C 116 (2012) 24962–24967.
[45] N. Ding, et al., Determination of the diffusion coefficient of lithium ions in nano-Si, Solid State Ionics 180 (2009) 222–225.
[46] M.A. Hopcroft, W.D. Nix, T.W. Kenny, What is the Young's modulus of silicon? J. Microelectromech. Syst. 19 (2010) 229–238.